Vorticity and entropy boundary conditions for acoustical finite-difference time-domain simulations

D. Botteldooren

Citation: The Journal of the Acoustical Society of America **102**, 170 (1997); doi: 10.1121/1.419780
View online: http://dx.doi.org/10.1121/1.419780
View Table of Contents: http://asa.scitation.org/toc/jas/102/1
Published by the Acoustical Society of America

Vorticity and entropy boundary conditions for acoustical finite-difference time-domain simulations

D. Botteldooren
Department of Information Technology, University of Gent, St. Pietersnieuwstraat 41, 9000 Gent, Belgium

(Received 7 February 1997; revised 15 March 1997; accepted 31 March 1997)

In this paper a time-domain numerical model for describing the presence of vorticity and entropy boundary layers is introduced. The boundary model can be inserted in acoustic time-domain models such as the finite-difference time-domain (FDTD) model for studying the acoustic behavior of high-quality resonator structures. The main focus in deriving the model is on numerical efficiency. Boundary layer theory is reviewed to obtain a three-dimensional formulation of its influence on FDTD equations that must be applied in boundary discretization cells. The $\sqrt{\omega}$ dependence that is encountered is approximated in time domain in such a way that no numerical convolution is required. Although this approximation is rather inaccurate, it is sufficient for most applications and introduces almost no extra computational effort. Several numerical examples illustrate the applicability of the model. © *1997 Acoustical Society of America.* [S0001-4966(97)05507-0]

PACS numbers: 43.20.Px, 43.20.Mv, 43.30.Gv [JEG]

INTRODUCTION

In highly resonant acoustic structures such as Helmholtz resonators, long hard ducts, strongly resonant enclosures, etc., absorption caused by the medium itself becomes important. In free air, molecular relaxation, viscosity and heat flux are important. In the presence of hard boundaries, absorption is often dominated by very thin layers near this boundary, called vorticity and entropy layers.[1] These layers are naturally incorporated in the solution of the wave equations that include viscosity and heat flux if appropriate boundary conditions are imposed. Solving the equations numerically leads to serious discretization problems because length scales of acoustic effects are typically several orders of magnitude larger than the boundary layer thickness. Using grid refinement near the boundary can solve the problem to some extent, but numerical cost remains considerable. In this paper it is therefore assumed that the boundary layer is much thinner than the typical grid cell required for the acoustic simulation, and a special boundary cell numerical model is introduced to take into account the influence of both vorticity and entropy layers.

First, boundary layer theory is reviewed. The mathematical theory starts from a formulation of the equations of linear acoustics in terms of acoustic pressure fluctuation p, acoustic density fluctuation ρ, and acoustic particle velocity $\mathbf{v}$. The equations include viscosity, heat flux, molecular rotational relaxation and molecular vibrational relaxation. It is preferred to stick with pressure and density to describe the absorption effects rather than to switch to the more usual entropy formulation for compatibility with linear acoustic studies in lossless media. When the boundary layer assumption is introduced in the derivation of the numerical model that can be applied in a boundary cell, a full three-dimensional description of boundary layer absorption emerges naturally.

The equations for the boundary cells have an important drawback. They include a $\sqrt{\omega}$ frequency dependence. An accurate transformation of this frequency dependence to time domain introduces a convolution. In general, this convolution must be evaluated numerically for each time step. This introduces an important calculation overhead. Recent papers in the field of electromagnetics[2,3] give some ideas on how to approximately solve the problem. Here the $\sqrt{\omega}$ frequency dependence is approximated by a combination of frequency domain functions that transform back to time-domain expressions that can more easily be evaluated numerically. The result is a numerical model for the boundary layer that requires only a very limited amount of additional CPU time.

The examples given at the end of this paper are mainly chosen to demonstrate the accuracy and applicability of the new boundary layer numerical formulation.

I. MATHEMATICAL MODEL

A. Equations of linear acoustics

To study the influence of vorticity and entropy boundary layers on the absorption of sound, an accurate free-field mathematical model must be used as a starting point. It is assumed that all boundaries of the acoustic environment that are studied are acoustically hard and that no material other than air is present in the simulation region. The frequency range of interest corresponds approximately to the audible frequency range. To cover this broad range several absorption mechanisms must be taken into account: fluid viscosity, heat flux, molecular rotational relaxation and molecular vibrational relaxation. Fluid viscosity μ influences the linearized Euler equation only.[1,4] It now reads

$$\rho_0 \frac{\partial \mathbf{v}}{\partial t} = -\nabla p + \frac{\mu}{3}\nabla(\nabla\cdot\mathbf{v}) + \mu\nabla^2\mathbf{v}, \tag{1}$$

where no static fluid flow is assumed, $\mathbf{v}$ is the acoustical particle velocity, p is the acoustic pressure, and ρ_0 is the density of air. Pierce[1] proves that the small departure of translational and rotational molecular kinetic energy from mutual thermodynamic equilibrium can be taken into account up to first order in acoustical quantities by introducing a bulk viscosity μ_B in Eq. (1). This gives

$$\rho_0 \frac{\partial \mathbf{v}}{\partial t} = -\nabla p + \left(\mu_B + \frac{\mu}{3}\right)\nabla(\nabla\cdot) + \mu\nabla^2\mathbf{v}. \tag{2}$$

The linearized conservation of mass equation is not changed by introducing the absorption mechanisms that are under consideration:

$$\frac{\partial \rho}{\partial t} = -\rho_0 \nabla\cdot\mathbf{v}. \tag{3}$$

To take into account sound absorption by heat conduction in the acoustic wave, nonadiabatic sound propagation must to be studied. This is often done by introducing acoustic entropy and temperature change as new variables.[1] Because sound pressure is much more often used for studying linear sound propagation, the energy conservation equation was transformed to a pressure equation that includes both the heat conduction and vibrational molecular relaxation terms in Ref. 4. In its linearized form the pressure equation reads

$$\frac{\partial p}{\partial t} = -\gamma p_0 \nabla\cdot\mathbf{v} + (\gamma-1)\kappa\nabla^2 T - (\gamma-1)\sum_i \frac{\rho_0 c_{vi}}{\tau_i} \times\left\{ T - \int^t T \exp\left(\frac{\tau - t}{\tau_i}\right)\frac{d\tau}{\tau_i}\right\}, \tag{4}$$

where γ is the ratio of specific heats, p_0 is the atmospheric pressure, κ is the coefficient of thermal conductivity, and T is the gas temperature (with vibrational molecular states frozen). The summation is over all types of molecules i present in the air gas mixture. The vibrational specific heat c_{vi} and the vibrational relaxation time τ_i can be obtained from absorption measurements and are found in literature. Since propagation Eqs. (3) and (4) for acoustic density and pressure are now different, acoustic density change will no longer be proportional to acoustic pressure change. Using the ideal gas law and the relation $\gamma p_0 = \rho_0 c^2$ between equilibrium pressure and equilibrium density, the gas temperature can be calculated in first order approximation as

$$T = \frac{p + p_0}{R(\rho + \rho_0)} \approx \frac{c^2}{\gamma R} + \frac{\gamma p - \rho c^2}{\gamma R \rho_0}. \tag{5}$$

Introducing this approximate value for T in Eq. (4) gives

$$\frac{\partial p}{\partial t} = -\gamma p_0 \nabla\cdot\mathbf{v} + \frac{(\gamma-1)}{\gamma R\rho_0}\kappa\nabla^2(\gamma p - \rho c^2) - \frac{(\gamma-1)}{\gamma R}\sum_i \frac{c_{vi}}{\tau_i}\left\{\gamma p - \rho c^2 - \int^t (\gamma p - \rho c^2) \times\exp\left(\frac{\tau - t}{\tau_i}\right)\frac{d\tau}{\tau_i}\right\}. \tag{6}$$

Since the absorption terms in Eq. (4) are small in free field and since ρ only influences the sound propagation through T, it is safe to assume $p = \rho c^2$ with first-order accuracy in the acoustic quantities, away from any boundaries. This approximation will easily be verified numerically in Sec. III. Introducing this approximation in Eq. (6) results in

$$\frac{\partial p}{\partial t} = -\gamma p_0 \nabla\cdot\mathbf{v} + \frac{(\gamma-1)^2}{\gamma R\rho_0}\kappa\nabla^2 p - \frac{(\gamma-1)^2}{\gamma R}\sum_i \frac{c_{vi}}{\tau_i}\left\{ p - \int^t p \exp\left(\frac{\tau - t}{\tau_i}\right)\frac{d\tau}{\tau_i}\right\}. \tag{7}$$

The set of equations (2) and (7) is sufficient to calculate sound propagation in free field, including all absorption mechanisms mentioned above and contains only $\mathbf{v}$ and p as unknown quantities. The numerical effort required to solve the set of equations is reduced considerably by this last approximation.

B. Vorticity and entropy boundary layer formulation

For simulations in linear acoustics it is sufficient to impose $\mathbf{v}\cdot\mathbf{n} = 0$ as a boundary condition when no absorption mechanisms are taken into account in Eqs. (2) and (6), where $\mathbf{n}$ is orthogonal on the surface. When viscosity and heat conduction terms are added to the equations for linear acoustics, assumptions must be made concerning tangential particle velocity and fluid temperature on the hard boundary. Three strategies can be considered:

(i) Real microscopic boundary conditions on a perfectly hard and heat conducting boundary imply that the tangential component of particle velocity is zero and the temperature near the boundary is equal to the constant surface material temperature. This approach implies that boundary layers are fully calculated and requires a very important numerical effort.

(ii) On the scale of acoustic wavelengths, boundary effects due to viscosity and heat conduction span only a very small region. Therefore, they are neglected in many circumstances. A corresponding boundary condition is

$$\frac{\partial \mathbf{v}_t}{\partial n} = 0 \quad \text{and} \quad \frac{\partial T}{\partial n} = 0, \tag{8}$$

where $\mathbf{v}_t$ is the tangential component of particle velocity. This approximation neglects all boundary absorption, which is the major sound absorption mechanism for highly resonant structures.

(iii) An analytical approach can be used for describing the vorticity and entropy boundary layers. The boundary condition for the acoustic simulation that is derived from this analytical approximation is the main subject of this paper.

The acoustic boundary layer theory[1] is based on the assumption that the solution of the full set of linear wave equations near a solid surface can be written as a superposition of an acoustic mode, an entropy mode and a vorticity mode. A solution for each of these fields is then found in the form of a plane wave: $\mathrm{Re}(\psi \exp(-j\omega t + j\mathbf{k}\cdot\mathbf{r}))$, where ω is the pulsation, $\mathbf{k}$ is the wave vector, and $\mathbf{r}$ is the spatial coordinate. For the vorticity and entropy part of the solution, the imaginary part of $\mathbf{k}$ is known to be quite large compared to the acoustic wave number in air. This means that vorticity and entropy fields must be localized near interfaces, surfaces and sources.

Based on this traditional theory it is assumed in this work that the total sound field very close to a flat acoustically hard surface only changes considerably in the direction n, which is orthogonal to this surface. As long as the boundary

layer is very thin compared to the wavelength of the sound and as long as the surface is flat on the same length scale, this is a good approximation. It is the only initial assumption that is made. The tangential velocity $\mathbf{v}_t$ at the boundary can be calculated by introducing this hypothesis in Eq. (2). This gives

$$\rho_0 \frac{\partial \mathbf{v}_t(n)}{\partial t} = \mu \frac{\partial^2 \mathbf{v}_t(n)}{\partial n^2}; \tag{9}$$

and the corresponding plane wave solution has the dispersion relation

$$k_n^2 = j\omega \frac{\rho_0}{\mu}, \tag{10}$$

where k_n is the orthogonal component of the wave vector $\mathbf{k}$. This dispersion relation, together with the condition that $\mathbf{v}_t = 0$ on the hard surface, completely describes the vorticity boundary field near the hard surface and will by used to obtain a special boundary cell in the numerical model.

To find a similar relation for the other acoustic quantities, the assumption that fields only change considerably in the n-direction is introduced in Eqs. (3) and (6) and in Eq. (2) for the v_n component only. Remark that Eq. (7) cannot be used since the assumption $p = \rho c^2$ is not valid in the boundary region. The resulting set of equations can be written in matrix form, where molecular relaxation effects have been omitted for simplicity since they do not contribute substantially to the boundary layer formation:

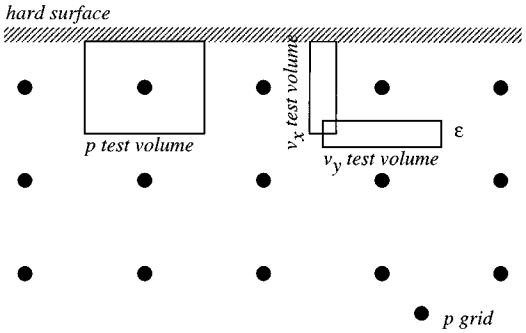

FIG. 1. Test volumes related to the unit cell that can be used to derive the FDTD equations.

$$\begin{pmatrix} \rho_0 \dfrac{\partial}{\partial t} - \left(\mu_B + \dfrac{4\mu}{3}\right)\dfrac{\partial^2}{\partial n^2} & \dfrac{\partial}{\partial n} & 0 \\ \gamma p_0 \dfrac{\partial}{\partial n} & \dfrac{\partial}{\partial t} - \dfrac{(\gamma-1)}{R\rho_0}\kappa\dfrac{\partial^2}{\partial n^2} & \dfrac{(\gamma-1)c^2}{\gamma R\rho_0}\kappa\dfrac{\partial^2}{\partial n^2} \\ \rho_0 \dfrac{\partial}{\partial n} & 0 & \dfrac{\partial}{\partial t} \end{pmatrix} \begin{pmatrix} v_n \\ p \\ \rho \end{pmatrix} = \begin{pmatrix} 0 \\ 0 \\ 0 \end{pmatrix}. \tag{11}$$

This set of equations has a nonzero solution only if the determinant of the first matrix is zero. After replacing the time derivative by $-j\omega$ and the spatial derivative by jk_n, a dispersion relation can be obtained that is of fourth order in k_n and of third order in ω. This equation can be solved for k_n^2 but the result is a rather complex function of ω. Taking into account the fact that μ, μ_B and κ are very small in air, two approximate solutions are found:

$$k_n^2 \approx \frac{\omega^2}{c^2} \quad \text{and} \quad k_n^2 \approx j\omega \frac{\gamma R \rho_0}{(\gamma-1)\kappa}. \tag{12}$$

The first relation describes the acoustic mode. Introducing this relation in Eq. (11) approximately gives the plane wave equations of linear acoustics with absorption neglected. The second dispersion relation describes the entropy field. From this relation and Eq. (11), it can be concluded that the entropy part of p must be very small. All field components v_n, p, and ρ show the same exponential behavior determined by this k_n in the entropy boundary region and so do all linear combinations of these fields. Of particular interest for the derivation of the numerical model is the combination $\gamma p - \rho c^2$ which is proportional to the change in temperature due to the sound wave as can be seen in Eq. (5). If the temperature of the hard surface can be assumed constant (and equal to the equilibrium temperature), then the quantity $\gamma p - \rho c^2$ is also zero on the surface. This completely describes the entropy boundary field.

II. NUMERICAL MODEL

A. General formulation

The numerical approximation to Eqs. (2) and (7) away from any boundary is based on a finite-difference time-domain (FDTD) discretization in a staggered grid.[5,6] In this paper the numerical approximation will be given in a Cartesian grid only. There is no fundamental problem in extending the implementation to a more general grid. The grid is described by the spatial steps δx, δy, and δz and the time step δt. In the following, a general spatial step is noted as $\delta\alpha$ and a spatial step orthogonal to a surface is noted as δn. Pressure p is discretized in locations given by integer multiples of the grid step; components of particle velocity are discretized in three staggered grids obtained by shifting this grid in the direction of the component that is considered, by half a grid step. Discretized pressure and particle velocity are determined at intermediate time, $t = \ell\,\delta t$ and $t = (\ell + 0.5)\,\delta t$, respectively.

The FDTD equations can be obtained by approximating all derivatives in Eqs. (2) and (7) by finite differences using a central difference scheme. An interesting alternative consists in integrating the analytic equations over well-chosen test volumes around the discretization locations. Suitable test volumes for pressure and particle velocity are shown in Fig. 1. Each approach leads to the set of FDTD equations

$$v_\alpha^{[\ell+0.5]}(\alpha+\tfrac{1}{2}) = v_\alpha^{[\ell-0.5]}\left(\alpha+\frac{1}{2}\right) - \frac{\delta t}{\rho_0\ \delta\alpha}(p^{[\ell]}(\alpha+1)-p^{[\ell]}) + \frac{\delta t(\mu_B+\mu/3)}{\rho_0\ \delta\alpha}(\psi^{[\ell]}(\alpha+1)-\psi^{[\ell]}) + \frac{\mu\,\delta t}{\rho_0}\chi_\alpha^{[\ell]}\left(\alpha+\frac{1}{2}\right), \tag{13}$$

and

$$p^{[\ell+1]} = p^{[\ell]} - \gamma p_0\ \delta t\ \psi^{[\ell+0.5]} + \frac{\kappa(\gamma-1)^2\ \delta t}{\gamma R\rho_0} \times \sum_\alpha \frac{p^{[\ell+0.5]}(\alpha+1)+p^{[\ell+0.5]}(\alpha-1)-2p^{[\ell+0.5]}}{\delta\alpha^2} - \frac{(\gamma-1)^2\delta t}{\gamma R\rho_0}\sum_i \frac{c_{vi}}{\tau_i}\{p^{[\ell+0.5]}-I_{\tau_i}^{[\ell+0.5]}\}, \tag{14}$$

with

$$\psi^{[\ell+0.5]} = \sum_\alpha \frac{v_\alpha^{[\ell+0.5]}(\alpha+\frac{1}{2})-v_\alpha^{[\ell+0.5]}(\alpha-\frac{1}{2})}{\delta\alpha}, \tag{15}$$

$$\chi_\alpha^{[\ell+0.5]}(\alpha+\tfrac{1}{2}) = \sum_{\alpha'} \frac{v_\alpha^{[\ell+0.5]}(\alpha+\frac{1}{2},\alpha'+1)+v_\alpha^{[\ell+0.5]}(\alpha+\frac{1}{2},\alpha'-1)-2v_\alpha^{[\ell+0.5]}(\alpha+\frac{1}{2})}{\delta\alpha'^2}, \tag{16}$$

where the index ℓ in square brackets is used for time discretization and where the spatial indices for the central pressure discretization location are omitted and spatial translation in the α-direction over $\delta\alpha/2$ is indicated as $(\alpha+\frac{1}{2})$. Summations over α run over the three Cartesian indices. A new variable I_{τ_i}, that contains the time integration up to now, is introduced. It can be calculated from the pressure p and its previous value at each time step as will be shown in Eq. (22). It is well known that a central difference approximation matches the staggered grid discretization completely for linear lossless sound propagation. Absorption terms in Eqs. (13) and (14) conserve the spatial match but introduce a time discretization mismatch; some quantities are needed at a moment in time where the are not calculated. An accurate and stable way to resolve this mismatch consists in interpolating linearly between the previously calculated value and the value that is calculated in the current time step. The drawback of this approach is that it interrelates the FDTD equations at different spatial locations. This increases the computational effort needed to solve the system of equations at each time step considerably. Since the terms involved are much smaller than the major terms in the FDTD equations, a less accurate approach seems sufficient. Two alternatives, which have comparable numerical accuracy, were tested. The first one consists in assuming that the unknown values are the same as the value $\delta t/2$ ago, which is known. The second one consists in extrapolating linearly to the future. The latter approach requires an increase in storage by about 50% but calculation time remains practically unchanged. Mainly because of the storage requirement, the first approximation is preferred. Stability analyses cannot be performed analytically. The approach is not unconditionally stable but since constants involved in the additional terms in the stability condition are always small, it can be assumed that the stability condition for lossless sound propagation $c\,\delta t < (1/\delta x + 1/\delta y + 1/\delta z)^{-1/2}$ is sufficient. This assumption is validated experimentally.

B. Special boundary cell formulation

In FDTD simulation, grid cells typically have a diameter that is about one tenth of the wavelength of the highest frequency of interest. In air, vorticity and entropy boundary effects typically span only a much smaller range even for the highest frequencies of interest. Therefore it is useful to try to incorporate the influence of the whole boundary layer on sound propagation in a single layer of special boundary cells. The derivation of the special FDTD equations for the boundary cell starts from Eqs. (2) and (6). These equations include first and second order derivatives of the unknown quantities. Only the derivatives orthogonal to the boundary are important if the boundary layer conditions stated in Sec. I B are fulfilled. The treatment of all field quantities is very similar. Therefore a description for a general field Ξ is given first. The field is assumed to be zero on the surface and to increase approximately exponentially away from the surface, so in the frequency domain

$$\Xi(n) \approx \Xi_0(1-e^{jk_n n}), \tag{17}$$

where k_n is the appropriate root from Eq. (10) or (12) and Ξ_0 is a constant. The discrete fields introduced in the previous section are easily interpreted as average values over the volume or surface of an elementary cell. Since Ξ is assumed to be constant in a plane parallel to the boundary, only an average over the n-direction will be important. If δn is the grid step in the n-direction this leads to

$$\frac{1}{\delta n}\int_0^{\delta n}\Xi(n)dn \approx \Xi_0\left(1-\frac{1}{jk_n\delta n}(e^{jk_n\delta n}-1)\right)\approx \Xi_0,$$

$$\frac{1}{\delta n}\int_0^{\delta n}\frac{\partial\Xi(n)}{\partial n}dn \approx -\frac{\Xi_0}{\delta n}(e^{jk_n\delta n}-1)\approx \frac{\Xi_0}{\delta n}, \tag{18}$$

$$\frac{1}{\delta n}\int_0^{\delta n}\frac{\partial^2\Xi(n)}{\partial n^2}dn \approx -\frac{jk_n\Xi_0}{\delta n}(e^{jk_n\delta n}-1)\approx \frac{jk_n\Xi_0}{\delta n},$$

where the last approximations are based on the assumption that $jk_n\delta n$ has a very large negative real part. This is the case if the grid cell is much larger than the boundary layer thickness. The first two relations in Eq. (18) can very easily be transformed back into time domain. The third relation poses a problem since both entropy layer and vorticity layer dispersion relations introduce a $\sqrt{\omega}$ frequency dependence through k_n.

Transforming this frequency dependence back to time domain is not an easy task. Recently Szabo[7] obtained a parabolic wave equation for lossy media obeying a general frequency power law. For the special case studied here (power $\frac{1}{2}$), his result requires a convolution in time domain with $t^{-3/2}$. The numerical implementation of this convolution requires a serious calculation effort at each time step and an important amount of additional storage. A less accurate, but more efficient approximation is required.

A time-domain approximation corresponding to the $\sqrt{\omega}$ dependence is obtained as a combination of a number of functions that can easily be implemented in time domain. In general the time-domain simulation is used to study signals that have a limited frequency content. Typically a frequency range of about one octave around a known central frequency f_0 is sufficient. Furthermore it is imposed that the absorption part of the approximation should not drop to zero at higher frequencies. High frequencies are not modeled accurately and some nonphysical absorption that eliminates them is appreciated. This is especially true if nonlinear effects are taken into account. Finally, the phase part can be approximated less accurately than the absorption part.

Frequency dependence that is easily implemented in time-domain models are low order integer powers of $j\omega$ or $1/j\omega$, and $1/(a-j\omega)$ which correspond to time derivatives, time integrations and a convolution with an exponential decay function in time domain, respectively. A comparison of different linear combinations of these basis functions learns that

$$-j\sqrt{j\omega}\approx C\frac{j\omega}{j\omega-1/\tau_0} \tag{19}$$

is a reasonable choice. In this approximation τ_0 is a relaxation parameter and C is a multiplier that can be used to tune the approximation. Figure 2(a) shows real and imaginary parts of the approximate frequency dependence for a fitted parameter set $\tau_0=1.2/\omega_0$ and $C=1.2\sqrt{\omega_0}$. The stars on the ω axes of this figure are the limits of the octave band around ω_0. For comparison a similar accuracy estimate is shown in Fig. 2(b) for Szabo's approach. A not sophisticated numerical integration based on the last 128 and 16 samples is used to evaluate the convolution. If sufficient samples are used

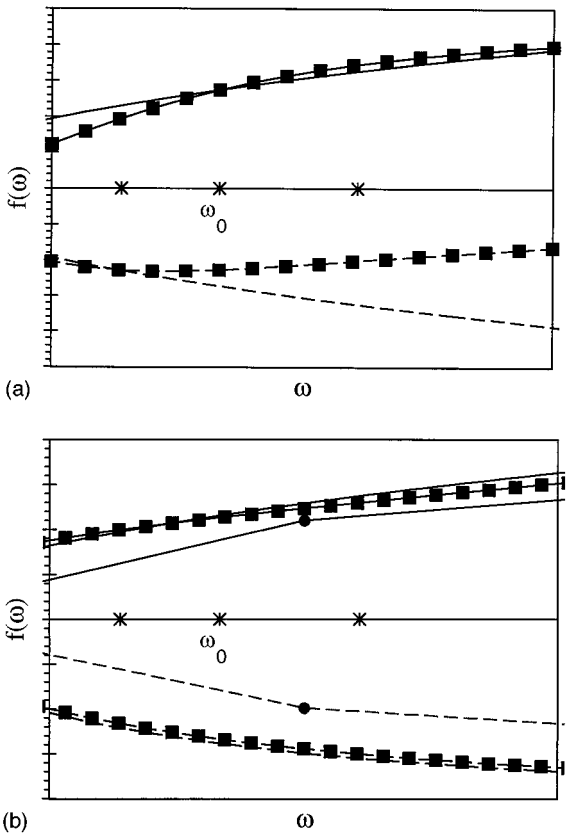

FIG. 2. Approximated frequency dependence (a) for the approximation used in this work (squares), (b) for the convolution approach using 128 (squares) and 16 (circles) past values; full line shows real part, dashed line shows imaginary part; stars limit one octave band

this approximation becomes very accurate as can be expected.

Based on the above approximation, the last equation of (18) can now be transformed back to time domain. Using the vorticity dispersion relation in Eq. (10) this leads to

$$\frac{1}{\delta n}\int_0^{\delta n}\frac{\partial^2\xi(n,t)}{\partial n^2}dn \approx -\frac{C}{\delta n}\sqrt{\frac{\rho_0}{\mu}}\left(\xi_0(t) - \frac{1}{\tau_o}\int_{-\infty}^{t}\xi_0(\tau)e^{(\tau-t)/\tau_0}\,d\tau\right), \tag{20}$$

where $\xi(n,t)$ and $\xi_0(t)$ are the time domain equivalents of $\Xi(n)$ and Ξ_0. To calculate the time integration numerically, a recursion formula can be found from

$$\frac{1}{\tau_o}\int_{-\infty}^{t+\delta t}\xi_0(\tau)e^{(\tau-(t+\delta t))/\tau_0}\,d\tau \approx \xi_0\left(t+\frac{\delta t}{2}\right)(1-e^{-\delta t/\tau_0}) + e^{-\delta t/\tau_0}/\tau_o\int_{-\infty}^{t}\xi_0(\tau)e^{(\tau-t)/\tau_0}\,d\tau, \tag{21}$$

where ξ_0 was assumed constant over a time interval δt. If the value of the integration up to $t=\ell\,\delta t$ is stored in the variable $I_{\tau_0}^{[\ell]}$ then the discrete form of Eq. (21) can be written as

$$I_{\tau_0}^{[\ell+1]} = \xi_0^{[\ell+1/2]}(1-e^{-\delta t/\tau_0}) + e^{-\delta t/\tau_0} I_{\tau_0}^{[\ell]}. \tag{22}$$

Special boundary cell FDTD equations can now be derived from Eqs. (2) and (6). Relevant changes to the FDTD Eqs. (14) and (13) can most easily be found by integrating (or averaging) the relevant acoustic equation over a well-chosen test volume. For the pressure equation (6) this test volume is the beam with dimensions δx, δy, and δz spanned around the discretization point (Fig. 1). At the left hand side of this equation, the pressure is averaged over the test volume. Equation (18) learns that this average is approximately equal to the value away from the boundary layer. The first term on the right hand side contains an integration of $\nabla \cdot \mathbf{v}$, which can be transformed to an integration of the orthogonal component of $\mathbf{v}$ over the closed surface of the test volume. On the different flat sub-surfaces this integration equals the unknown components of the particle velocity, which include entropy and vorticity fields. In particular on the hard surface $v_n = 0$ can be used to first order. The summation over molecular vibration resonances contains only averaging of p and ρ over the test volume. They can be approximated as shown in Eq. (18) by the value away from the boundary. Therefore it is also possible to calculate ρ in this part of the equation by using the relation $p = \rho c^2$. The second term on the right-hand side contains an average of $\nabla^2(\gamma p - \rho c^2)$ over the test volume. As was argued in Section I B, $(\gamma p - \rho c^2)$ changes primarily in the direction orthogonal to the boundary so the derivatives parallel to this boundary can safely be neglected compared to the orthogonal derivative. The average of the second order derivative orthogonal to the boundary of $(\gamma p - \rho c^2)$ can be calculated by substituting $\xi(n,t)$ by $(\gamma p - \rho c^2)$ in the equivalent of Eq. (20) for the entropy layer. The quantity $\xi_0(t)$ now corresponds to the value of $(\gamma p - \rho c^2)$ away from the boundary, which is equal to $(\gamma - 1)p$. Taking into account these remarks a first FDTD equation for a boundary cell is obtained

$$\begin{aligned} p^{[\ell+1]} = p^{[\ell]} &- \gamma p_0 \, \delta t \, \psi^{[\ell+0.5]} \\ &- \frac{(\gamma-1)C}{\delta n}\sqrt{\frac{(\gamma-1)\kappa}{\gamma R \rho_0}}(p^{[\ell+0.5]} - I_{\tau_0}^{[\ell+0.5]}) \\ &- \frac{(\gamma-1)^2}{\gamma R \rho_0}\sum_i \frac{c_{vi}}{\tau_i}\{p^{[\ell+0.5]} - I_{\tau_i}^{[\ell+0.5]}\}, \end{aligned} \tag{23}$$

where Eq. (21) with ξ_0 replaced by p is used to update $I_{\tau_0}^{[\ell+0.5]}$ and $I_{\tau_i}^{[\ell+0.5]}$ every time step and ψ is defined in Eq. (15).

Equation (2) must be studied separately for the orthogonal and for the parallel component of the particle velocity. A flat test volume of height ϵ located around each surface of the test volume used to derive the pressure equation can be used (Fig. 1). All terms in Eq. (2) applied to one component of the particle velocity are integrated over the appropriate test volume. The time derivative on the left-hand side reduces to the time derivative of the discretized unknown velocity: the orthogonal component averaged over a surface of the pressure test volume. The volume integration of the first and second term on the right-hand side can be transformed to an integration over the surface surrounding the test volume.

TABLE I. Absorption (/m) in a long duct for different spatial discretization steps.

$\delta\alpha$	FDTD simulation	Analytical	Relative difference
$\lambda/14$	2.22×10^{-4}	2.47×10^{-4}	9.97%
$\lambda/28$	2.34×10^{-4}	2.47×10^{-4}	5.22%
$\lambda/56$	2.41×10^{-4}	2.47×10^{-4}	2.46%

The contribution of the small sides of the test volume is zero since these surfaces are orthogonal to the velocity component that is considered. The integration over the two larger surfaces introduces a gradient of p and $\nabla \cdot \mathbf{v}$. Both can be calculated from the assumption that p and $\nabla \cdot \mathbf{v}$ vary linearly between known values in the center of the adjacent pressure test volumes. Boundary layers only influence these terms indirectly through p and $\nabla \cdot \mathbf{v}$. The last term on the right-hand side must be studied more carefully. For a parallel component of particle velocity v_α the test volume clearly crosses the boundary layer. The average of the second order derivative orthogonal to the boundary can be calculated by substituting $\xi(n,t)$ by v_α in Eq. (20), since v_α is zero on the boundary and decays according to dispersion relation (10) as explained in Sec. I B. The quantity $\xi_0(t)$ now corresponds to the value of v_α away from the boundary. Second-order derivatives parallel with the surface are neglected since they are much smaller than the orthogonal derivative. Taking into account these remarks, the FDTD equation for a component v_α parallel with the surface, in a boundary cell is obtained

$$\begin{aligned} v_\alpha^{[\ell+0.5]}(\alpha+\tfrac{1}{2}) = v_\alpha^{[\ell-0.5]}(\alpha+\tfrac{1}{2}) &- \frac{\delta t}{\rho_0 \, \delta\alpha}(p^{[\ell]}(\alpha-1) - p^{[\ell]}) \\ &+ \frac{\delta t\left(\mu_B + \dfrac{\mu}{3}\right)}{\rho_0 \, \delta\alpha}(\psi^{[\ell]}(\alpha+1) - \psi^{[\ell]}) \\ &+ \frac{C \, \delta t}{\delta n}\sqrt{\frac{\mu}{\rho_0}}(v_\alpha^{[\ell]} - J_{\tau_0}^{[\ell]}), \end{aligned} \tag{24}$$

where Eq. (21) with ξ_0 replaced by v_α is used to update $J_{\tau_0}^{[\ell]}$ every time-step and ψ is defined in Eq. (15).

The orthogonal component v_n is zero on the surface so no time stepping is required. To calculate the discretized component of v_n at a distance δn from the surface, the standard FDTD equation (13) can be used. The discretized approximation of the second order derivative uses the surface value of v_n, which is assumed to be zero. Although this is a very poor approximation for the second order derivative in this case, the error on viscous damping that this approxima-

TABLE II. Absorption (/m) in a long duct for different values of the central frequency in the narrow-band excitation.

f	FDTD simulation	Analytical	Relative difference
$f_0/2$	0.92×10^{-4}	1.64×10^{-4}	43.9%
f_0	2.34×10^{-4}	2.47×10^{-4}	5.22%
$2f_0$	4.43×10^{-4}	3.81×10^{-4}	−16.5%

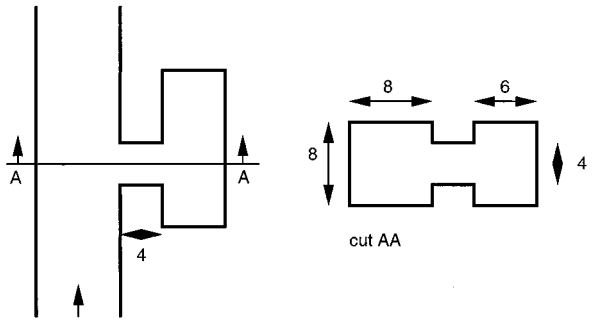

FIG. 3. Structure of the Helmholtz resonator on a duct used in the example (sizes in cm).

tion introduces is always small compared to the large damping that is present in the adjacent boundary pressure cell. Therefore it can safely be used.

In Eqs. (23) and (24) all spatial inconsistencies are resolved. Inconsistency in time discretization is again approximately resolved by linear extrapolation.

III. NUMERICAL RESULTS

A. One-dimensional test cases

To evaluate the accuracy of the numerical model that is described in this paper, sound propagation in a long, quasi one-dimensional duct is studied numerically and compared to known analytical results.[1] Since these analytical results are based on a number of approximations, they cannot be considered as an absolute reference. All numerical simulations described in this section will be performed with a test signal that is limited both in frequency content and in time

$$g(t)=A\ \sin(2\pi f(t-t_0))e^{-(t-t_0)^2/\sigma^2}, \tag{25}$$

where A is the amplitude, f is the central frequency, t_0 is some initial delay, and σ determines both bandwidth and signal duration. For the simulations in this section $\sigma=1.6/f$. A typical frequency of interest f_0 is chosen and boundary layer approximations are based on this frequency. The diameter of the duct that is studied is $\lambda_0/3.4$ and its length is $4.5\lambda_0$ where λ_0 is the wavelength corresponding to the frequency f_0. The duct is terminated with perfectly reflecting boundaries at both ends.

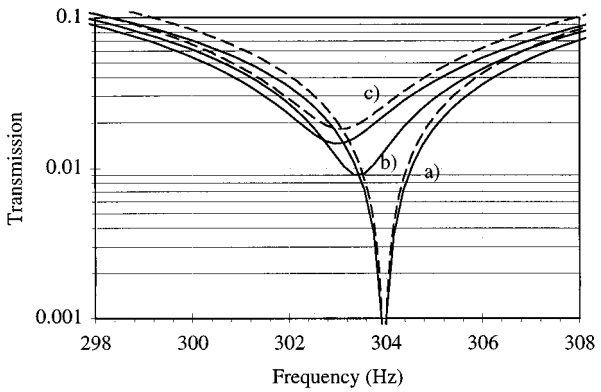

FIG. 4. Resonance peak in the transmission corresponding to the lowest order resonance of the resonator; (a) no boundary layer; (b) vorticity layer included; (c) vorticity and entropy layer included; dashed lines are results of the analytical model.

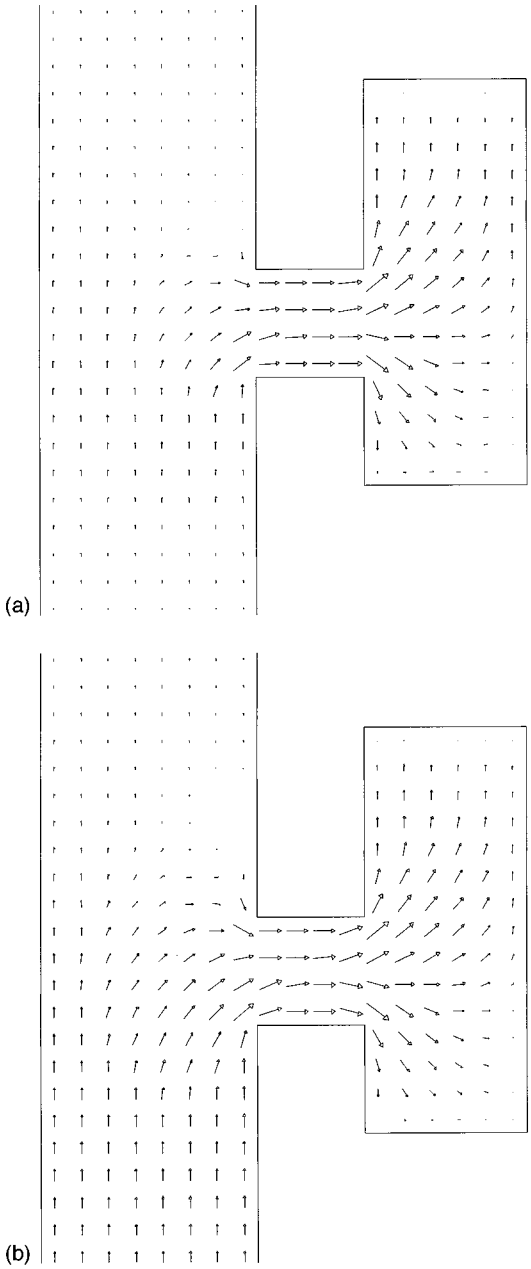

FIG. 5. Vector sound intensity in the plane of the resonator; (a) without boundary layer effects; (b) with boundary layer effects included.

First the inaccuracy introduced by the assumption $p=\rho c^2$ is investigated. This is done by comparing simulation results of the model presented in this paper to results obtained with a model that discretizes Eqs. (2), (3), and (6). The relative difference between both simulation results remains within 0.5% for simulated time up to 10 seconds or corresponding propagation distance of 3.4 km. This is clearly sufficient. Moreover such a small difference can easily be due to different numerical error in both implementations.

A strong point of the vorticity and entropy boundary layer formulation that is introduced in this paper is its numerical efficiency. An increase of 6.5% in CPU-time requirement for boundary cells was observed after introducing

the new boundary formulation. Since boundary cells normally occupy less than 10% of the simulation region, this is indeed an insignificant increase in CPU-requirements.

FDTD results for a bandlimited signal with central frequency f are compared to analytical predictions for a single frequency corresponding to f for different spatial discretization steps ($\delta x = \delta y = \delta z$) in Table I. Absorption was measured by calculating the rms value of the finite length time signal at different instances near one end of the duct. The simulation was done for $f = f_0 = 50$ Hz so the boundary layer thickness can have no influence on the results in the table. The relative difference in absorption coefficients decreases approximately linear with spatial discretization step and is typically below 5%. The same behavior was observed for frequencies up to 20 kHz. Considering the fact that several minor effects such as finite duct length and finite bandwidth were neglected in the analytical model, this result is quite promising.

The previous numerical test does not measure the accuracy of the approximate frequency dependence of the boundary layer effect that is introduced in Eq. (19). Keeping f_0 and spatial discretization fixed, the central frequency f of the excitation was detuned. In Table II numerical results are again compared to analytical approximations. Away from f_0 numerical error increases. As can be expected from Fig. 2, the error is much more important for lower frequencies. This limitation of the model should be kept in mind. Fortunately in practical situations where vorticity and entropy boundary layers are important, the frequency band of interest is rather small since highly resonant structures are studied.

B. High quality resonator

The second simulation example is a high quality resonator placed on a duct. Two resonator modes are investigated: the traditional lowest-order resonance and a first-order mode in the resonator, parallel to the duct. The structure is shown in Fig. 3. Frequency-domain transmission change is found by FFT transform of the time-domain response for a wavelet excitation. For the lowest-order resonance an approximate analytical model is available.[8] One of the parameters in the model is the neck end correction. Since this parameter cannot be calculated analytically for the structure that is modeled here, it is fitted in order to match the resonance frequency obtained with the FDTD model to that obtained with the analytical model, for the lossless case. Figure 4 shows the lowest order resonance in the transmission change simulated with the FDTD model if no boundary layers are included, if only the vorticity layer is included and if both vorticity and entropy layer are included. FDTD results are obtained with $f_0 = 300$ Hz. The dashed line is the transmission change calculated with the analytical model with and without absorption effects. FDTD results and analytical results correspond quite well. Remember however that the resonator neck end correction that was used in the analytical model is a fitted parameter. The model presented here can be used to determine this parameter for several resonator configurations.

Interesting distributions of acoustical quantities can be displayed to analyze the influence of the boundary layer absorption in greater detail. Vector sound intensity averaged over 50 periods in the plane of the resonator is shown in Fig. 5. The duct is excited with a pure tone tuned exactly to the resonance frequency of the resonator. If boundary layer effects are neglected, there is no difference between duct energy flux before and after the resonator. If boundary absorption is included a clear energy transport from the source to the resonator is observed.

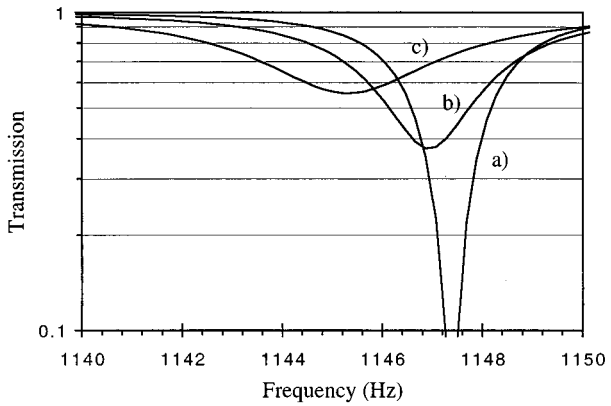

FIG. 6. Resonance peak in the transmission corresponding to the first longitudinal resonance in the resonator; (a) no boundary layer; (b) vorticity layer included; (c) vorticity and entropy layer included.

The first longitudinal resonance of the resonator occurs at a frequency of 1150 Hz. The corresponding resonance in the transmission change is shown in Fig. 6 as obtained by the FDTD simulation. For these simulations $f_0 = 1200$ Hz. Three situations are again compared: no boundary layer, vorticity layer only, and both vorticity and entropy layer. The influence of the boundary layers on the resonance peak is slightly different than in the previous case. The reason for this difference can be found in the fact that the absorption caused by the vorticity and the entropy boundary layer depend in a different way on the direction of incidence of the acoustic wave. Absorption by the vorticity layer is larger for shear sound propagation while absorption by the entropy layer is independent on direction of the sound propagation.

IV. CONCLUSIONS

A new numerical time-domain model that describes the influence of vorticity and entropy boundary layers on sound propagation is introduced. The model can very efficiently be included in a finite-difference time-domain simulation of acoustic problems. The computational overhead is very small. Numerical accuracy is sufficient for the problems that require the use of such a model.

ACKNOWLEDGMENT

The author is a senior research assistant with the Belgian National Fund for Scientific Research.

[1] A. D. Pierce, *Acoustics* (McGraw-Hill, New York, 1981).

[2] F. Torres, P. Vaudon, and B. Jecko, ''Application of fractional derivatives to the FDTD modeling of pulse propagation in a Cole–Cole dispersive medium,'' Microw. Opt. Technol. Lett. **13**, 300–304 (1996).

[3] R. J. Luebbers and F. Hunsberger, ''FDTD for *n*th-order dispersive media,'' IEEE Trans. Antennas Propag. **40**, 1297–1301 (1992).

[4] D. Botteldooren, ''Numerical model for moderately non-linear sound propagation in three dimensional structures,'' J. Acoust. Soc. Am. **100**, 1357–1367 (1996).
[5] K. S. Kunz and R. J. Luebbers, *The Finite Difference Time Domain Method for Electromagnetics* (CRC, Boca Raton, 1993).
[6] A. Taflove, *Computational Electrodynamics: The Finite-Difference Time-Domain Method* (Artech House, Boston, MA, 1995).
[7] T. L. Szabo, ''Time domain wave equations for lossy media obeying a frequency power law,'' J. Acoust. Soc. Am. **96**, 491–500 (1994).
[8] F. P. Mechel and I. L. Vér, ''Sound-absorbing materials and sound absorbers,'' in *Noise Control*, edited by L. L. Beranek and I. L. Vér (Wiley, New York, 1992).